Construction and Building Materials 200 (2019) 318–323

Contents lists available at ScienceDirect

Construction and Building Materials

journal homepage: www.elsevier.com/locate/conbuildmat

Pore structure development during hydration of tricalcium silicate by X-ray nano-imaging in three dimensions

Bo Chen [a,b,c,*], Wei Lin [a], Xianping Liu [a,c,*], Francesco Iacoviello [d], Paul Shearing [d], Ian Robinson [a,b,e]

[a] School of Materials Science and Engineering, Tongji University, Shanghai 201804, China
[b] London Centre for Nanotechnology, University College London, London WC1H 0AH, UK
[c] Key Laboratory of Advanced Civil Engineering Materials (Tongji University), Ministry of Education, Shanghai 201804, China
[d] Electrochemical Innovation Laboratory, Department of Chemical Engineering, University College London, London WC1E 6BT, UK
[e] Department of Condensed Matter Physics and Materials Science, Brookhaven National Laboratory, Upton, NY 11973, USA

HIGHLIGHTS

- Pore structure development of a hydrating C_3S was revealed by X-ray Nano-CT;
- The shape, size/volume and spatial distribution of the pores was revealed in 3D;
- The sealed pores grow larger and the open pores become smaller during the hydration.

ARTICLE INFO

Article history:
Received 26 July 2018
Received in revised form 13 December 2018
Accepted 20 December 2018

Keywords:
Tricalcium silicate hydration
X-ray nano-computed tomography (X-ray Nano-CT)
Three-dimensional structure
Pore structure
Cement

ABSTRACT

Tricalcium silicate (C_3S) is the most important component among the four main clinker phases of Portland cement. Pure C_3S is widely used as a simplified model system of cement in various researches. However, the spatial structure development of cement, even pure C_3S during hydration at the nano-scale has been rarely directly reported. In this work, X-ray nano-computed tomography (X-ray Nano-CT), a non-destructive X-ray analytical method, was used to study the hydration of a pure C_3S sample with a water/C_3S mass ratio of 0.5. The three-dimensional (3D) structure of the hydrating C_3S specimen was investigated to see the internal pore structure evolution within the hardened C_3S paste. Investigation of the 3D structural development of the C_3S specimen at different hydration times was performed to monitor the changes of pore shapes and sizes/volumes. It is found that volumes of the sealed pores generally grow larger, and the open pores become smaller while the volume and the external morphology of the whole hardened C_3S paste remains almost the same during hydration.

1. Introduction

The chemical reactions of Portland cement with water determine the setting and hardening behavior of the cement mortar and cement concrete, as well as the overall structure of these materials [1–4]. The internal spatial structure or morphologic organization produced by these hydration reactions has been widely investigated in order to understand their impact on the setting and hardening process of the cement-based materials, and later on the properties and performance of these hardened materials. Research has shown that the morphologic organization of cement-based materials has great impact on their mechanical and engineering properties and performance, sometimes even more important than their chemical composition [5–10]. In the cement-based materials, the pore structure is a critical factor that determines the internal morphologic organization. Hence the pore structure directly affects the key properties and performance of cement-based materials such as their impermeability, shrinkage, elastic modulus and strength [11,12]. Tricalcium silicate ($3CaO{\cdot}SiO_2$, or simplified as C_3S), as the most important constituent of Portland cement clinker, has been extensively investigated [13–17] because its hydration controls the setting and strength development of the cement-based materials. In our study, C_3S was used as a simplified model system of cement to investigate the internal pore structure development of the sample during the hydration process.

Direct observation of changes in the microstructure of cement-based materials is challenging for many experimental techniques.

* Corresponding authors at: School of Materials Science and Engineering, Tongji University, Shanghai 201804, China.
E-mail addresses: bo.chen@tongji.edu.cn (B. Chen), lxp@tongji.edu.cn (X. Liu).

https://doi.org/10.1016/j.conbuildmat.2018.12.120
0950-0618/

So far, the microstructure of cement paste has been widely studied in order to have a better understanding of the cement hydration process, and thus to develop better and more-dedicated cement-based materials [18–23]. However, there are few reports on the internal pore structure of cement paste, especially at the nano-scale [24–27]. This is partly because the cement paste is extremely complex and disordered, and partly because three-dimensional (3D) imaging techniques are needed for completing the measurements. Although it is hard to precisely measure the porosity of cement paste, there are 3 methods are usually used to estimate its quantity: gas adsorption [28], mercury intrusion porosimetry (MIP) [29] and direct observation techniques including optical microscopy and scanning electron microscopy (SEM) [30–32]. Gas absorption and MIP only provide indirect measurements of the pore structure. SEM, which is frequently used to characterize the cement materials, usually can only show the pores in two dimensions. However, it has not been reported making direct observation of the evolution of the structure of cement paste over time by these techniques in three dimensions. What is more, these techniques require dedicated sample preparation that may also introduce artifacts.

According to all the work have been completed so far, there is still no agreement reached about the detailed mechanisms of cement hydration due to the lack of sufficiently detailed experimental observations, especially the observations of the temporal evolution of the microstructure of cement-based materials [33–36]. This paper presents the use of X-ray nano-computed tomography (X-ray Nano-CT) to directly observe the morphological evolution of a cement paste model, a hydrating pure C_3S paste, as a function of hydration time in order to enrich our knowledge of the underlying hydration mechanism at the nano-scale in three dimensions.

2. Experiments

X-ray Nano-CT is a 3D imaging technique that uses a transmission X-ray microscopy (TXM) instrumental setup as shown in Fig. 1. In our investigation, a Zeiss Xradia 810 Ultra, an X-ray Nano-CT instrument with capabilities to reach 50 nm resolution in three dimensions, was used to record the projections of the target objects. Similar to a traditional CT machine, this X-ray Nano-CT records the projections as a function of rotation angle in the forward transmission geometry, and uses a Fresnel Zone Plate (FZP), after the sample, as a projective lens with high magnification (see Fig. 1). It then reconstructs a 3D image from the acquired projections using a filtered back-projection (FBP) CT algorithm. Although Zernike phase contrast (ZPC) [37] imaging mode is available from the X-ray Nano-CT we used by inserting a phase ring in it [38,39], considering the possibly unnecessary artifacts introduced by ZPC, in the work reported here, phase ring was removed from the X-ray Nano-CT. The absorption contrast only projections were collected to observe the spatial microstructure of a hydrated pure C_3S paste in three dimensions.

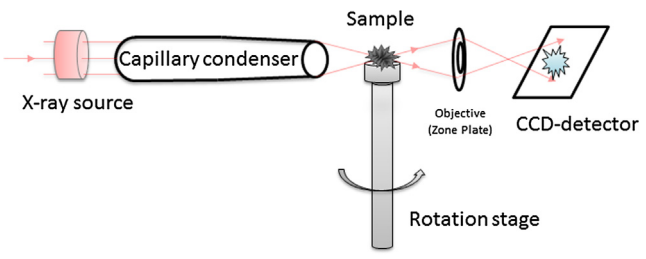

Fig. 1. A schematic diagram of the X-ray nano-computed tomography (X-ray Nano-CT) setup.

Pure monoclinic C_3S was synthesized at Tongji University by following the experimental procedure reported by De la Torre & Aranda [40]. The synthesized bulk specimen was stored in a small sealed box at room temperature with desiccant. It was later crashed and ground into very fine powder. The C_3S powder was then mixed with water at a water/C_3S weight ratio of 0.5. The fresh C_3S paste was injected into a thin-wall glass capillary tube with an inner diameter of 100 μm. It should be pointed out that the injection tends to bring more water into the capillary. After that, the specimen was sectioned immediately to a length of about 1 mm to avoid capillary effects. These short sections of the paste were then sealed into two layers of resealable plastic bags, and then were placed into a waterproof lock-and-seal plastic container box for curing under 23 °C. After 5 days of curing, the hydrated C_3S samples were taken out from the resealable bag. Because of the limitation of the field of view (FoV) of the X-ray Nano-CT, about 64 μm × 64 μm, the capillaries that are containing the samples were carefully cracked, the hydrated C_3S particles were taken out by steel scalpel. The particles with possibly suitable sizes were then glued to sharp pins and checked by very quick X-ray Nano-CT measurements. At last, one of the hydrated C_3S particles with most suitable size was selected and mounted to the X-ray Nano-CT sample holder for the first full measurement. After the measurement, this hydrating C_3S paste sample was kept in a sealed box for curing again till 28 days in a 22–23 °C atmosphere with about 55% humidity. Then, it was measured again by the X-ray Nano-CT under the same conditions.

During the X-ray Nano-CT measurements, the instrument cabinet temperature was stably kept at 27–28 °C. The sample was mounted on a stage with four degrees of freedom: x, y and z translations for positioning and a rotation stage for tomographic data acquisition. The X-ray Nano-CT uses a microfocus rotating Chromium anode X-ray source (Rigaku MicroMax-007HF) operated at 35 kV and 25 mA with an resulting operating power of 0.875 kW. The generated illumination X-rays are quasi-monochromatic X-rays with an energy of 5.4 keV (Cr-Ka radiation), and the focal spot size FWHM (full width at the half maximum) is 75 μm ± 11 μm. The focus was done by a full-reflection glass capillary condenser lens. The used detector is a 1024 × 1024 pixels 16-bit Peltier-cooled CCD camera with a physical pixel size of 13.5 μm × 13.5 μm. For each 3D tomographic measurement, the sample was rotated from −90° to 90° with 0.25° interval, totally 720 absorption contrast only projections of the sample in each measurement was recorded for the 3D reconstruction. The exposure time for each projection is 60 s, and the total acquisition time (including detector reading-out time) for each tomographic measurement is a bit more than 12 h.

3. Results and discussions

3.1. General analysis of the structure of the C_3S paste

Fig. 2 shows the reconstructed cross-sectional images of the hydrated C_3S paste specimen at 2 hydration times. Fig. 2a and 2b present 2 cross-sectional images of the sample after 5 days of hydration from different orientations; Fig. 2d and 2e also present the cross-sections of the same sample after 28 days of hydration from different orientations. Fig. 2c and 2f are the segmented images of Fig. 2b and 2e, respectively, using the 3D image analysis software package Avizo (Avizo, Thermo Fisher Scientific, Waltham, Massachusetts, USA). The dark parts seen in the non-segmented cross-sectional images in Fig. 2 are “empty” space, and all the white parts are the solid phases in the hydrated C_3S paste. These white parts in Fig. 2a, b, d and e have higher density. They are

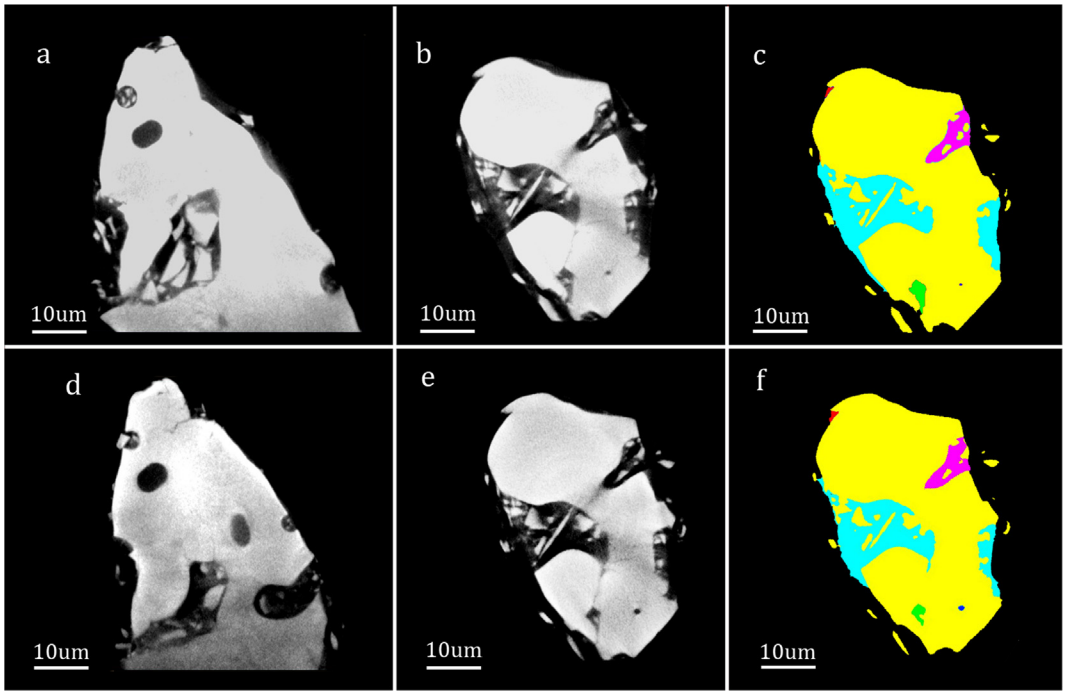

Fig. 2. Reconstructed cross-sectional images of the hydrated C_3S paste from X-ray Nano-CT. (a, b) Cross-sectional images of the hydrated C_3S paste after 5 days of hydration from 2 different orientations; (c) Segmented result of b; (d, e) Cross-sectional images of the hydrated C_3S paste after 28 days of hydration; (f) Segmented result of e. The yellow parts in panels c and f are the solid hydration products and the unhydrated C_3S particles in the sample. The purple, light blue, green and red colored parts in panels c and f are pores inside the sample. (For interpretation of the references to colour in this figure legend, the reader is referred to the web version of this article.)

the solid hydration products and the unhydrated C_3S particles that are colored as yellow in Fig. 2c and f. For the large dark part surrounding the specimen (i.e. the solid phases of the sample), it is atmosphere; for those black parts inside the specimen, they are pores. The pores inside the specimen are colored in Fig. 2c and f as purple, light blue, green and red etc.

Fig. 3 presents the rendered images of the reconstructed volume of the specimen. For both hydration times, we can clearly see the whole morphology and internal structure of the C_3S paste in three dimensions. The 3D spatial distribution of the pores inside the specimen are shown in Fig. 3b, c, e and f. The volumes of segmented pores and solid phase are calculated by the software Avizo,

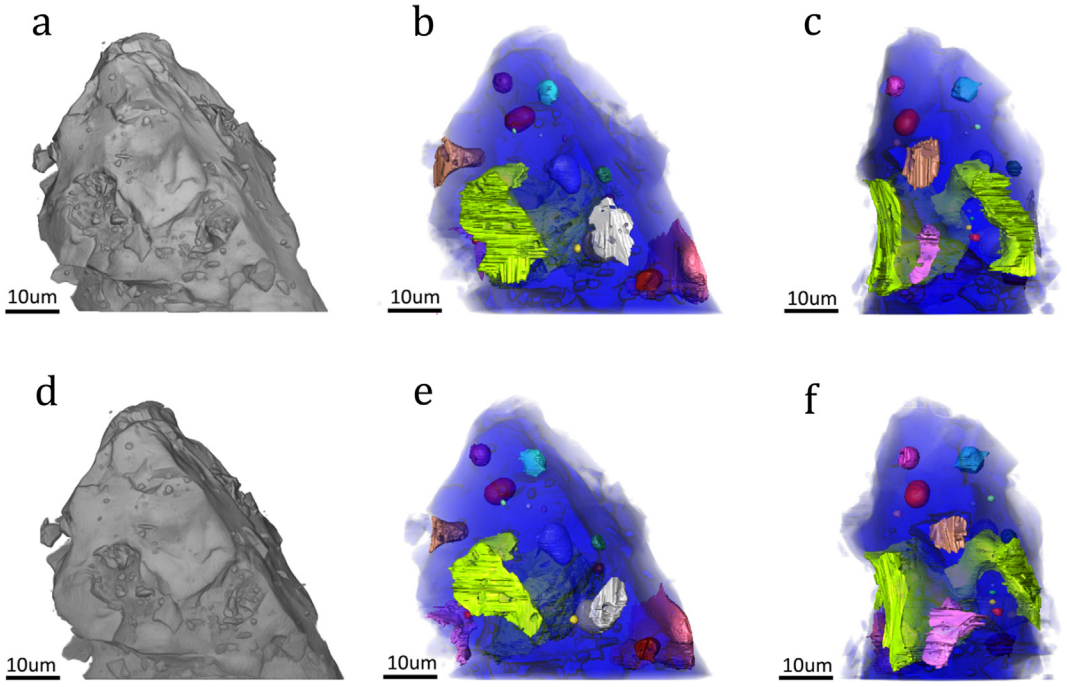

Fig. 3. Rendering of the 3D volume images of the hydrated C_3S paste specimen. (a) Surface rendering of the specimen structure after 5 days of hydration, (b) & (c) Transparent rendering of the segmented 3D image in panel a from 2 different orientations (d) Surface rendering of the specimen structure after 28 days of hydration, (e) & (f) Transparent rendering of the segmented 3D image in panel d from 2 different orientations.

and the results are presented in Table 1. Generally, from outside, the shape of the whole C_3S paste specimen looks very similar at both hydration times. From Table 1, it can be seen that the total volume of the sample (solid and pores) remains almost the same, increased from 45,162 um^3 (after 5 days of hydration) to 45,214 um^3 (after 28 days of hydration), with only about 0.1% change. This confirms that during the hardening process (after final setting) of the cement, the outside shape of the paste keeps almost the same. The volume fraction of pores was seen to decrease as the hydration time went from 5 days to 28 days with a clear change from 9.82% to 9.13%.

Previous research has suggested that the hydration process occurs not only on the surface, but also inside the cement paste, even the techniques used in most of this work cannot resolve the specific location where the hydration happens and is only roughly quantitative [41,42]. Our result shows a clear evolution of shape and spatial distribution of each pore, which will be discussed in detail later.

3.2. Spatial distribution and shape analysis of the pores

Fig. 4 presents 3D renderings of the pores only (after segmentation). We identified 21 pores in total after removing all the pores smaller than 64 voxels ($4 \times 4 \times 4$ voxels). They are named as pore A to U, from large to small, and the large ones from A to K are labeled in Fig. 4. Pores with different sizes and shapes could be clearly seen, and they scatter within the sample which cannot be visualized in 2D slice images or by traditional 2D imaging techniques. There are two types of pores in the measured paste volume: sealed pores that are totally surrounded by C_3S paste, and open pores that have at least one path exposed to the atmosphere. In the measured volume, pores E, F, I, L, M, N, O, R, S, T and U are sealed ones, and the others could be treated as open pores. Pore A, the largest pore in our measured sample, is crossing through the whole sample, and becomes longer and narrower as the hydration time goes on from 5 days to 28 days. The sealed pores are found to be distributed randomly within the specimen, and they seem not to change much either in shape or size by first eye sight while the hydration goes on.

While the spatial arrangement of pores is clearly shown in Fig. 4, we still cannot easily identify the evolution of the position of each pore during hydration. To clarify these changes, the centers of mass of all the pores were calculation by using Avizo after 3D image segmentation. Their distances to pore E were presented in Fig. 5. It shows clearly that the relative pore positions within the hydrated paste barely changed during hydration, which is consistent with the similar image appearance of these pores in Fig. 4a and 4b.

Table 1
The volume analysis of the C_3S paste at both hydration times.

	Porosity (%)	Solid phases (um^3)	Pores (um^3)
5 days	9.82	40,725	4437
28 days	9.13	41,083	4130

3.3. Microstructure quantification

The quantitative analysis result of the 21 pores found in the specimen after hydration for 5 days and 28 days are presented in Table 2 in terms of the morphological parameters including Feret length(L), Feret width(W) and volume(V) that are calculated by using Avizo. The volume change of pores (in percentage) between the two hydration times is also shown in Table 2. Since the images were segmented semi-automatically with manual operations, they may contain interpretation errors introduced inevitably. For a higher accuracy of the subsequent analysis and discussion of the pore structure, we took out the pores with the highest and the lowest value of volume change, pore H and pore D, respectively, in our consideration.

It found that all the sealed pores, E, F, I, L, M, N, O, P, Q, R, S, T and U, grow bigger via the hydration goes on. Almost all the open pores, except for pore J, become smaller. Pore A, an open pore and the largest pore in the observed volume, looks grow longer and narrower in Fig. 4, and it becomes smaller (shrunken 14%) via hydration, see Table 2. This obvious volume reduction of pore A dominates the volume change of the pores within the specimen

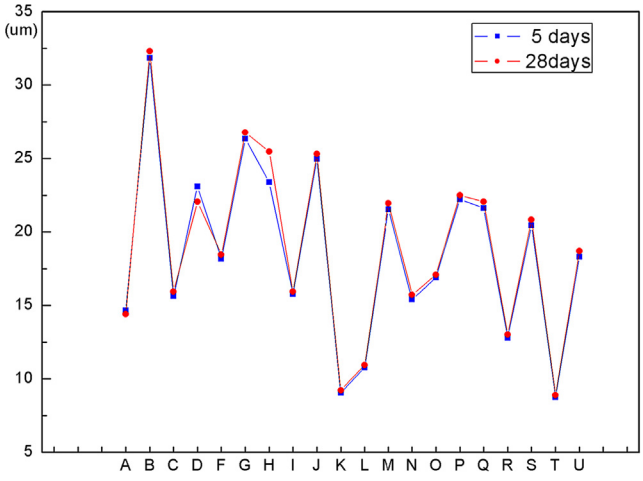

Fig. 5. Distances of the pores to the pore E in the C_3S paste specimen measured after hydration for 5 days and 28 days.

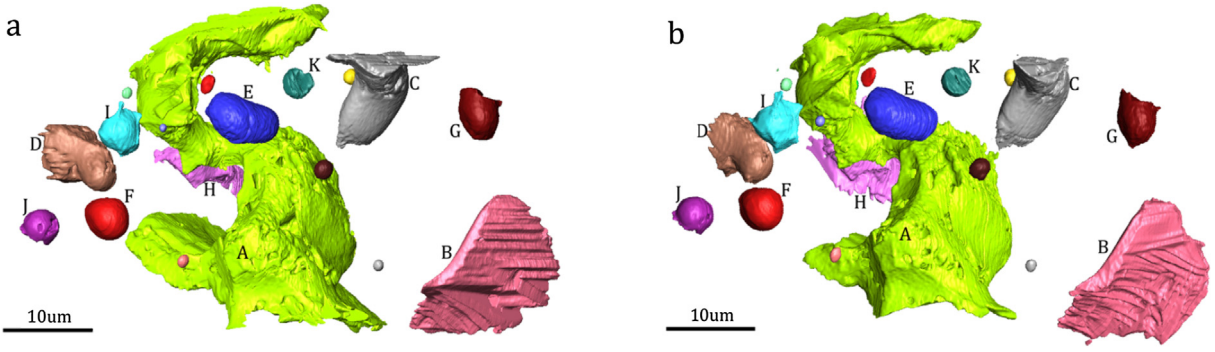

Fig. 4. Rendering of 3D spatial structure images of the pores within the C_3S paste specimen after hydration for (a) 5 days and (b) 28 days.

Table 2
Pore size of C_3S after hydration for 5 days and 28 days.

		5 Days				28 Days			Change in V(%)
		L(μm)	W(μm)	V(μm^3)		L(μm)	W(μm)	V(μm^3)	
1	A	43.1	26.0	2980.8	A	45.5	24.5	2625.6	−14
2	B	22.1	10.8	615.1	B	22.8	11.7	605.2	−02
3	C	17.2	8.9	278.7	C	15.9	7.5	244.5	−14
4	D	12.0	7.8	158.8	D	10.1	6.8	93.7	−70
5	E	8.4	5.0	122.8	E	9.0	5.5	136.9	+10
6	F	6.4	4.5	73.1	F	6.5	4.8	80.6	+09
7	G	6.7	5.1	55.3	G	8.6	4.9	49.1	−12
8	H	13.3	6.6	52.3	H	18.4	8.5	166.0	+69
9	I	6.9	4.3	47.8	I	10.8	5.3	63.7	+25
10	J	5.0	3.8	24.3	J	7.4	4.4	32.7	+26
11	K	3.8	2.8	12.4	K	4.0	2.7	12.3	−01
12	L	2.5	2.1	5.2	L	2.9	2.3	6.8	+24
13	M	2.5	1.6	2.8	M	2.8	1.7	3.1	+10
14	N	2.0	1.7	2.6	N	2.4	1.9	3.2	+17
15	O	1.7	1.2	1.2	O	2.0	1.2	1.6	+21
16	P	1.5	1.2	1.0	P	1.8	1.3	1.3	+24
17	Q	1.4	1.1	0.7	Q	1.5	1.1	0.7	+01
18	R	1.4	1.0	0.7	R	3.7	1.4	1.2	+41
19	S	1.6	1.0	0.6	S	1.3	1.1	0.6	+00
20	T	1.1	0.9	0.4	T	1.4	1.2	0.9	+57
21	U	1.1	0.8	0.3	U	1.7	0.9	0.5	+43

since it is much larger than all the other pores. Pore C, an open pore as well, has similar change as pore A. For the open pore B, both its length and width increased. However, its volume turns out to be decreased, which means its height/diameter becomes smaller and there are hydration products occupying its internal space. Pore G, another open pore, has close width at 2 different hydration times with increased length via hydration goes on, and its volume decreases as well. Similar to pore B, this means its internal space was occupied by the hydration products while the time goes.

The sample were prepared with sufficient water to allow the hydration reaction to continue during the whole experiment. For the water-accessible open pores within the hydrating C_3S specimen, the hydration products will continue to grow and fill the "empty" space within the pores. So, their volumes decreased while the hydration went on. Another result of the growth of the hydration products is the volume increase of the whole solid phases of the hardened C_3S paste sample (Table 1). On the other hand, the volume growth of the sealed pores over time should be caused by the autogenous chemical shrinkage. Because the hydrating C_3S or cement paste under sealed conditions will self-desiccate, this creates empty pores or extra space in the existing pores within the hydrating paste due to loss of water [43]. Once the hydration products formed during the hydration occupied less "empty" space than the corresponding amount of "empty" space/pores created by the loss of water at the same time, the chemical shrinkage would happen [44]. Although pore J is an open pore in the observed volume, however, it is very similar to a sealed pore with little space open to the atmosphere (see Fig. 4), and this could make pore J behave like a sealed pore rather than an open pore.

From these results, obvious pore structure change could be observed. However, compared with a regular hydrating C_3S or cement sample with a water/C_3S or water/cement ratio at 0.5, the structure evolution is quite less visible. This was very likely caused by the loss of water of the hydrated C_3S sample during the X-ray measurements, especially after the continuous long-time X-ray tomographic measurements. Because the X-ray illumination will heat-up the sample locally and cause the water evaporation which would lead to the decrease of water/C_3S ratio of the measured sample and hence slow down the hydration of the C_3S. As the sample was kept in a sealed box and surrounded by air for curing, not kept in a humid environment or water again after the first X-ray tomographic measurement, so, its hydration was happening at a slow rate between the 2 tomographic measurements.

4. Conclusions

X-ray nano-computed tomography (X-ray Nano-CT) is shown to be a powerful tool for the non-destructive investigation of the porosity structure of cement-based materials such as the hydrating C_3S paste. The laboratory-based X-ray Nano-CT could observe the slow structural evolution over a relatively long time period associated with such as C_3S or cement hydrating and hardening. The work demonstrates the detailed morphological information on shape, size/volume and spatial distribution of the pores within the hydrating C_3S paste. These pores within the hydrating C_3S paste particle changed significantly as the hydration went on from 5 days to 28 days, while the external morphology of the measured C_3S paste particle including its shape and volume remained almost unchanged. X-ray Nano-CT provides 3D images of the internal structure of the measured specimens, as required to understand the development of the pore microstructure within the cement-based materials. It was further found that the relative position of each pore shows little change during the hydration process in our experiment. Importantly, there is a general trend that the volumes of sealed pores within the hydrating paste grow larger, and the open pores usually become smaller during the hydration process, which confirms that the growth of hydrates within the hardened C_3S or cement paste would fill in the "empty" space of the open pores during continued hydration.

On the other hand, the work shows that the X-ray illumination tends to lead to the loss of water in the hydrating C_3S or cement paste, and slow down their hydration process.

Acknowledgment

This work was supported by the High-level Talent Program "Materials Nanostructure" with grant numbers 152221 and 152243 from Tongii University, "Shanghai PuJiang Talent Program" with grant number 18PJ1410400, and the UK Engineering and Physical Sciences Research Council (EPSRC) grant EP/I022562/1 "Phase modulation technology for X-ray imaging". Work performed at Brookhaven National Laboratory was supported by the US Depart-

ment of Energy, Office of Basic Energy Sciences, under Contract Number DE-SC00112704. Part of the work at Tongji University was also supported by the National Natural Science Foundation of China with grant number 51102181. The authors also thank Andrew Chiu for helping with the measurements.

Conflicts of interest

The authors declare no conflict of interest.

References

[1] P. Barnes, J. Bensted, Structure and performance of cements, Edition 2, Chapter3, CRC Press: pp. 57–113 (2002)
[2] H.F.W. Taylor, Cement chemistry, Edition 2, Thomas Telford, 1997.
[3] E.M. Gartner, J.M. Gaidis, Hydration Mechanisms I, in Materials Science of Concrete, Edited by J. Skalny, American Ceramic Society, Westerville, OH 1 (1989) 95–125.
[4] J.W. Bullard, H.M. Jennings, R.A. Livingston, A. Nonat, G.W. Scherer, J.S. Schweitzer, K.L. Scrivener, J.J. Thomas, Mechanisms of cement hydration, Cem. Concr. Res. 41 (2011) 1208–1223.
[5] I. Maruyama, Y. Nishioka, G. Igarashi, K. Matsui, Microstructural and bulk property changes in hardened cement paste during the first drying process, Cem. Concr. Res. 58 (2014) 20–34.
[6] M.S. Sumanasooriya, N. Neithalath, Stereology- and morphology-based pore structure descriptors of enhanced porosity (pervious) concretes, ACI Mater. J. 106 (5) (2009).
[7] J. Hu, Porosity of concrete, morphological study of model concrete PhD thesis, Delft University, the Netherlands, 2004.
[8] N. Neithalath, A. Marolf, J. Weiss, J. Olek, Modeling the influence of pore structure on the acoustic absorption of enhanced porosity concrete, J. Adv. Concr. Technol. 3 (2005) 29–40.
[9] S. Lu, E.N. Landis, D.T. Keane, X-ray microtomographic studies of pore structure and permeability in Portland cement concrete, Mater. Struct. 39 (2006) 611–620.
[10] Q. Chen, H.H. Zhu, J.W. Ju, F. Guo, L.B. Wang, et al., A Stochastic Micromechanical model for Multiphase Composite Containing Spherical Inhomogeneities, Acta Mech. 226 (6) (2015) 1861–1880.
[11] T.C. Hansen, Physical structure of hardened cement paste: a classical approach, Mater. Struct. 19 (6) (1986) 423–436.
[12] Y. Xi, D.D. Siemer, B.E. Scheetz, Strength development hydration reaction and pore structure of autoclaved slag cement with added silica fume, Cem. Concr. Res. 27 (27) (1997) 75–82.
[13] P.A. Slegers, M. Genet, A.J. Léonard, J.J. Fripiat, Structural transformation of tricalcium silicate during hydration, Appl Cryst 10 (1977) 270–276.
[14] H.F.W. Taylor, P. Barret, P.W. Brown, et al., The hydration of tricalcium silicate, Mater. Struct. 17 (1984) 457–468.
[15] L.S. Dent Glasser, E.E. Lachowski, K. Mohan, H.F.W. Taylor, A multi-method study of C3S hydration, Cem. Concr. Res. 8 (6) (1978) 733–739.
[16] R.A. Livingston, J.S. Schweitzer, C. Rolfs, H.W. Becker, S. Kubsky, Characterization of the induction period in tricalcium silicate hydration by nuclear resonance reaction analysis, Mater. Res. 16 (3) (2001) 687–693.
[17] D. Damidot, F. Bellmann, B. Möser, T. Sovoidnich, Calculation of the dissolution rate of tricalcium silicate in several electrolyte compositions, Cem Wapno Beton 12 (2) (2007) 57–67.
[18] L. Holzer, P.H. Gasser, A. Kaech, M. Wegmann, A. Zingg, R. Wepf, B. Muench, Cryo-FIB-nanotomography for quantitative analysis of particle structures in cement suspensions, J. Microsc-Oxford 227 (2007) 216–228.
[19] J.C. da Silva, P. Trtik, A. Diaz, et al., Mass Density and Water Content of Saturated Never-Dried Calcium Silicate Hydrates, Langmuir 31 (2015) 3779–3783.
[20] A. Cuesta, A.G. De la Torre, I. Santacruz, et al., Chemistry and mass density of aluminum hydroxide gel in Eco-Cements by Ptychographic X-ray computed tomography, Phys. Chem. C 121 (2017) 3044–3054.
[21] D.P. Bentz, Three-dimensional computer simulation of Portland cement hydration and microstructure development, J. Am. Ceram. Soc. 1 (1997) 3–21.
[22] W. Suna, K. Houa, Z. Yanga, Y. Wenb, X-ray CT three-dimensional reconstruction and discrete element analysis of the cement paste backfill pore structure under uniaxial compression, Constr. Build. Mater. 138 (2017) 69–78.
[23] Q. Hu, M. Aboustait, T. Kim, M. Tyler Ley, J.C. Hanan, J. Bullard, R. Winarski, V. Rose, Direct three-dimensional observation of the microstructure and chemistry of C_3S hydration, Cem. Concr. Res. 88 (2016) 157–169.
[24] T. Pavel, D. Ana, G. Manuel, M. Andreas, B. Oliver, Density mapping of hardened cement paste using ptychographic X-ray computed tomography, Cem. Concr. Compos. 36 (2013) 71–77.
[25] B. Nathan, C. Perrine, V. Jérôme, B. Daniel, L. Clément, et al., Micro- and nano-X-ray computed-tomography: a step forward in the characterization of the pore network of a leached cement paste, Cem. Concr. Res. 67 (2015) 138–147.
[26] W. Yan-Shuai, D. Jian-Guo, X-ray computed tomography for pore-related characterization and simulation of cement mortar matrix, NDT&E International 86 (2017) 28–35.
[27] A. Cuesta, A.G. De la Torre, I. Santacruz, P. Trtik, J.C. da Silva, et al., In-situ hydration imaging study of a ye'elimite paste by ptychographic X-ray computed tomography, in: Proceedings of the 39th International Conference on Cement Microscopy, International Cement Microscopy Association, Toronto: 17-32 (2017)
[28] M. Juenger, H. Jennings, The use of nitrogen adsorption to assess the microstructure of cement paste, Cem. Concr. Res. 31 (2001) 883–892.
[29] A.B. Abell, K.L. Willis, D.A. Lange, Mercury intrusion porosimetry and image analysis of cement-based materials, J. Colloid Interface Sci. 211 (1999) 39–44.
[30] J.E. Bailey, H.R. Stewart, C_3S hydration products viewed using a cryo stage in SEM, J. Mater. Sci. Lett. 3 (5) (1984) 411–414.
[31] F.V. Lawrence, J.F. Young, Studies on the hydration of tricalcium silicate pastes: I. Scanning electron microscopic examination of microstructural features, Cem. Concr. Res. 3 (2) (1973) 149–161.
[32] H.M. Jennings, B.J. Dalgleish, P.L. Pratt, Morphological development of hydrating tricalcium silicate as examined by electron microscopy, J. Am. Ceram. Soc. 64 (10) (1981) 567–572.
[33] J.W. Bullard, G.W. Scherer, J.J. Thomas, Time dependent driving forces and the kinetics of tricalcium silicate hydration, Cem. Concr. Res. 74 (2015) 26–34.
[34] G.W. Scherer, J. Zhang, J.J. Thomas, Nucleation and growth models for hydration of cement, Cem. Concr. Res. 42 (2012) 982–993.
[35] J.J. Thomas, J.J. Biernacki, J.W. Bullard, S. Bishnoi, J.S. Dolado, G.W. Scherer, A. Luttge, Modeling and simulation of cement hydration kinetics and microstructure development, Cem. Concr. Res. 41 (2011) 1257–1278.
[36] J.W. Bullard, A determination of hydration mechanisms for tricalcium silicate using a kinetic cellular automation model, J. Am. Ceram. Soc. 91 (2008) 2088–2097.
[37] F. Zernike, Phase contrast, a new method for the microscopic observation of transparent objects, Physica 9 (7) (1942) 686–698.
[38] U. Neuhäusler, G. Schneider, W. Ludwig, M.A. Meyer, E. Zschech, D. Hambach, X-ray microscopy in Zernike phase contrast mode at 4keV photon energy with 60nm resolution, J. Phys. D Appl. Phys. 36 (2003) 79–82.
[39] I. Vartiainen, R. Mokso, M. Stampanoni, C. David, Halo suppression in full-field x-ray Zernike phase contrast microscopy, Opt. Lett. 39 (6) (2014) 1601–1604.
[40] A.G. De la Torre, M.A.G. Aranda, Accuracy in Rietveld quantitative phase analysis of Portland cements, J. Appl. Cryst. 36 (2003) 1169–1176.
[41] M.C.G. Juenger, P.J.M. Monteiro, E.M. Gartner, G.P. Denbeaux, A soft X-ray microscope investigation into the effects of calcium chloride on tricalcium silicate hydration, Cem. Concr. Res. 35 (2005) 19–25.
[42] D.A. Silva, P.J.M. Monteiro, The influence of polymers on the hydration of Portland cement phases analyzed by soft X-ray transmission microscopy, Cem. Concr. Res. 36 (2006) 1501–1507.
[43] D.P. Bentz, O.M. Jensen, Mitigation strategies for autogenous shrinkage cracking, Cem. Concr. Compos. 26 (6) (2004) 677–685.
[44] E. Tazawa, S. Miyazawa, T. Kasai, Chemical shrinkage and autogenous shrinkage of hydrating cement paste, Cem. Concr. Compos. 25 (2) (1995) 288–292.